Supporting Information

Ppb-Level, Dual Channel Sensing of Cyanide and Bisulfate Ions in Aqueous Medium: Computational Rationalization of Ion-Dependent ICT Mechanism

Suvendu Paul, Rikitha S Fernandes, Nilanjan Dey*

* Department of Chemistry, BITS Pilani, Hyderabad Campus, Telangana-560078, India.
E-mail: nilanjan@hyderabad.bits-pilani.ac.in
ORCID Id: SP: 0000-0001-9544-0102, ND: orcid.org/0000-0002-3988-1509

Synthesis and Characterization

General Procedure for the Preparation of Oxidized Di(indolyl)arylmethanes (1-3). To a mixture of 4-substituted benzaldehyde (1.0 equiv), indole (2.0 equiv), I_2 (0.05-0.10 equiv) in methanol (4 mL) a methanolic solution of DDQ (1.0 equiv) was slowly added dropwise over a period of 15-20 min at rt. The precipitate often appeared after addition of DDQ and it was kept for sometime to settle the precipitate. The precipitate was filtered and washed consequently with methanol and EtOAc and then dried under vacuo.[1]

3-[(2,3-Dihydro-1*H*-indol-3-yl)-*p*-tolyl-methylene]-3*H*-indole (1). Yield 90%; Green crystals, mp 237-238 ℃ (decompose); IR (KBr, cm^{-1}) 3432.7, 3106.8, 2200.6, 1607.5, 1531.4, 1479.7, 1410.3, 1372.9, 1327.7, 1241.3, 1176.5, 1123.2, 745.3; ^{1}H NMR (400 MHz, CD$_3$OD): δ 2.57 (s, 3H), 6.90 (d, *J* = 8.0 Hz, 2H), 7.13 (t, *J* = 7.6 Hz, 2H), 7.38 (t, *J* = 7.6 Hz, 2H), 7.5 (d, *J* = 8 Hz, 2H), 7.57 (d, *J* = 8 Hz, 2H), 7.65 (d, *J* = 8.0 Hz, 2H), 8.25 (s, 2H), NH is not seen; ^{13}C NMR (100 MHz, DMSO-d_6) δ 21.2, 97.7, 115.4, 116.8, 120.9, 122.5, 123.1, 125.0, 127.5, 129.5, 130.7, 132.0, 136.0, 142.2, 143.6, 146.9, 159.5; TLC R$_f$ = 0.28 (5% MeOH/CHCl$_3$); MS(ESI) *m/z* 335(M+H)$^+$; HRMS *m/z* calcd for C$_{24}$H$_{19}$N$_2$ (M+H)$^+$ 335.1548, found 335.1541.

4-[(1*H*-Indol-3-yl)-indol-3-ylidene]-nitrobenzene (2). After completion of the reaction as indicated by TLC solvent was evaporated under vacuo. The residue was acidified with dil. HCl (pH ~4) and gray solid was obtained on filtration. The solid residue was then thoroughly washed with EtOAc and dried under vacuo. Yield 50%; Brown solid, mp 233-235 ℃ (decompose); IR (KBr, cm^{-1}) 3450.3, 2202.3, 1581.3, 1523.4, 1479.1, 1407.7, 1348.0, 1172.5, 1116.5, 759.8; ^{1}H NMR (400 MHz, CD$_3$OD) δ 6.83-6.87 (m, 4H), 7.05 (t, *J* = 7.4 Hz, 2H), 7.13 (t, *J* = 7.6 Hz, 2H), 7.29-7.40 (m, 8H), 7.65 (d, *J* = 8.4 Hz, 2H), 7.85-7.88 (m, 4H), 8.07 (d, *J* = 8.8 Hz, 2H), 8.3 (s, 2H), 8.47 (d, *J* = 8.8 Hz, 2H); ^{13}C NMR (100 MHz, DMSO-d_6) δ 115.5, 120.9, 122.5, 123.4, 123.8, 125.3, 126.8, 127.8, 129.7, 132.5, 143.7, 144.9, 147.4, 148.9; TLC R$_f$ = 0.51 (5% MeOH/CHCl$_3$); MS(ESI) *m/z* 366 (M+H)$^+$; HRMS *m/z* calcd for C$_{23}$H$_{16}$N$_3$O$_2$ (M+H)$^+$ 366.1242, found 366.1244.

{4-[(1H-Indol-3-yl)-indol-3-ylidene-methyl]-phenyl}-*N,N$^{/}$*-dimethylaminobenzene(3). After completion of the reaction as indicated by TLC solvent was evaporated under vacuo. The solid obtained after washing the residue was successively washed with (3 × 2) mL of EtOAc and MeOH. Yield 60%; Red solid, mp 244-245 ℃ (decompose); IR (KBr, cm^{-1}) 3438.4, 2198.4, 1602.5, 1488.7, 1415.4, 1378.8, 1182.1, 1116.5, 750.1; ^{1}H NMR (400 MHz, CD$_3$OD) δ 3.28 (s, 6H), 6.99 (t, *J* = 8.8 Hz, 4H), 7.09 (t, 2H), 7.33 (t, *J* = 8.0 Hz, 2H), 7.62 (d, *J* = 8.0 Hz, 2H), 7.67 (d, *J* = 8.4 Hz, 2H), 8.01 (s, 2H); ^{13}C NMR (100 MHz, DMSO-d_6) δ 112.2, 115.1, 120.8, 121.0, 122.9, 124.7, 125.5, 127.9, 136.7, 142.5, 144.6, 154.5, 160.3; TLC R$_f$ = 0.28 (5% MeOH/CHCl$_3$); MS(ESI) *m/z* 364 (M+H)$^+$; HRMS *m/z* calcd for C$_{25}$H$_{22}$N$_3$ (M+H)$^+$ 364.1813, found 364.1811.
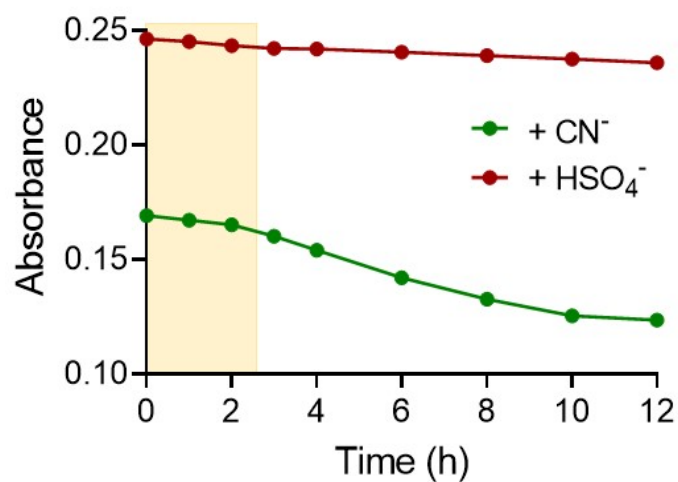
Additional Spectral Data

Fig S1. Time-dependent changes in absorbance of **1** in presence of CN⁻ (at 435 nm) and HSO$_4^-$ ions (at 525 nm) in water medium.
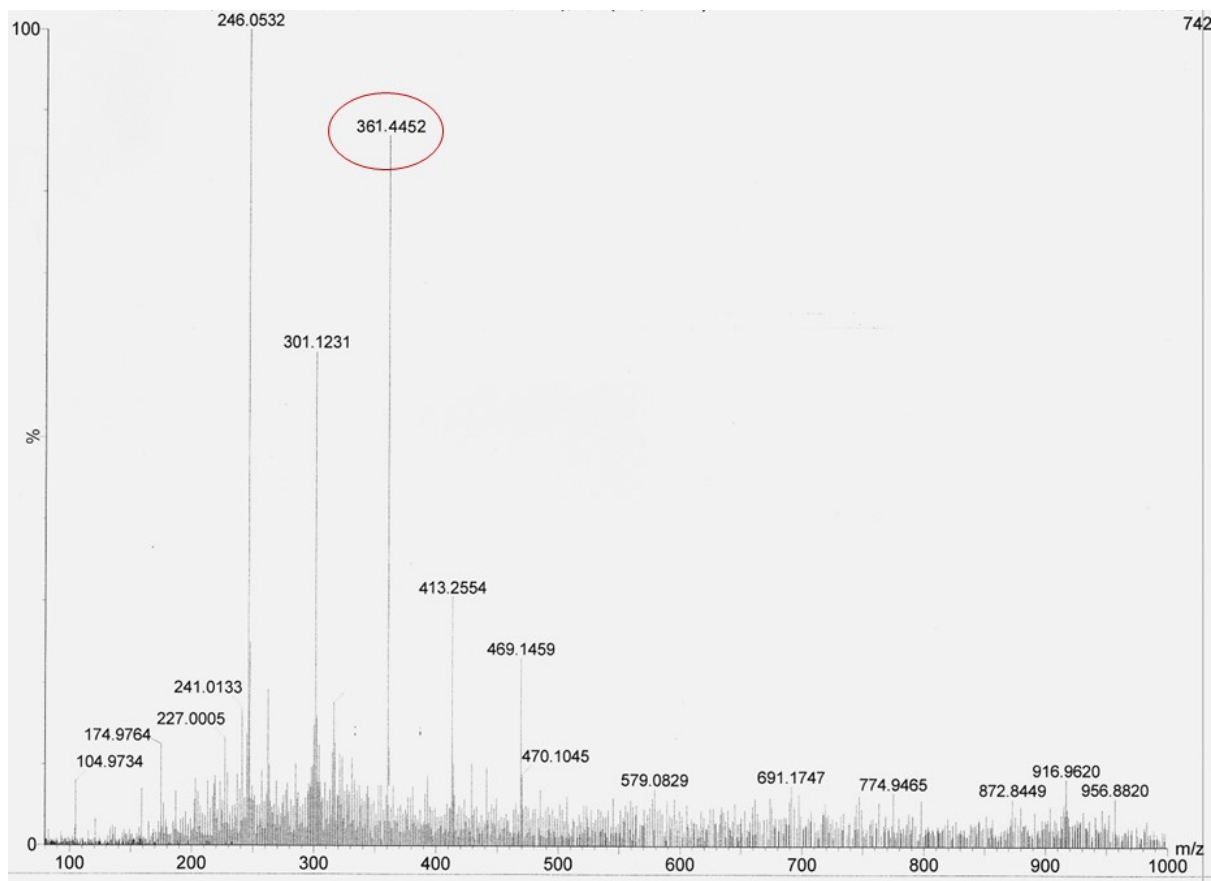

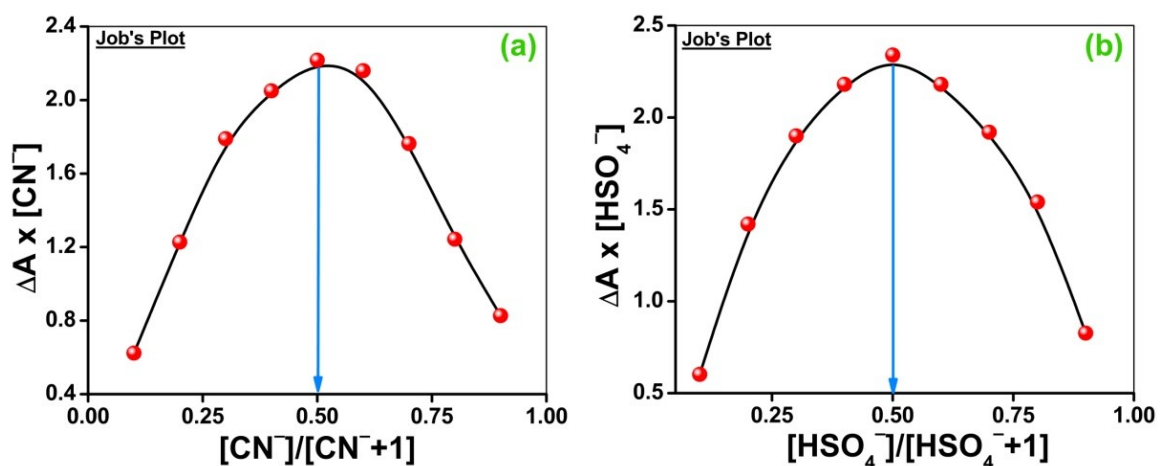**Fig S2.** HRMS mass spectrum of **1** with CN⁻ ions after 24 h.

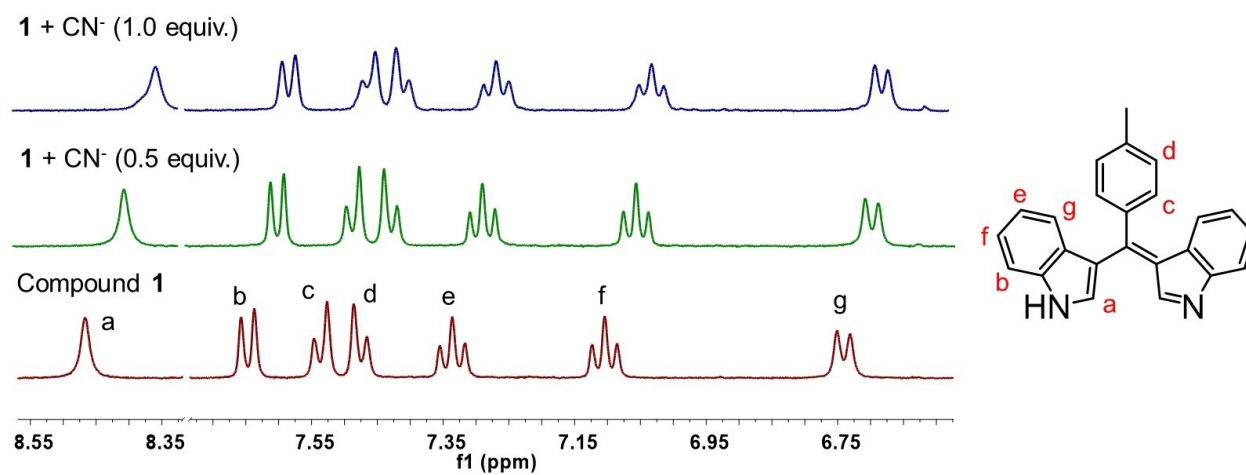**Fig S3.** Job's plots of **1**-CN⁻ (a) and **1**-HSO₄⁻ (b).

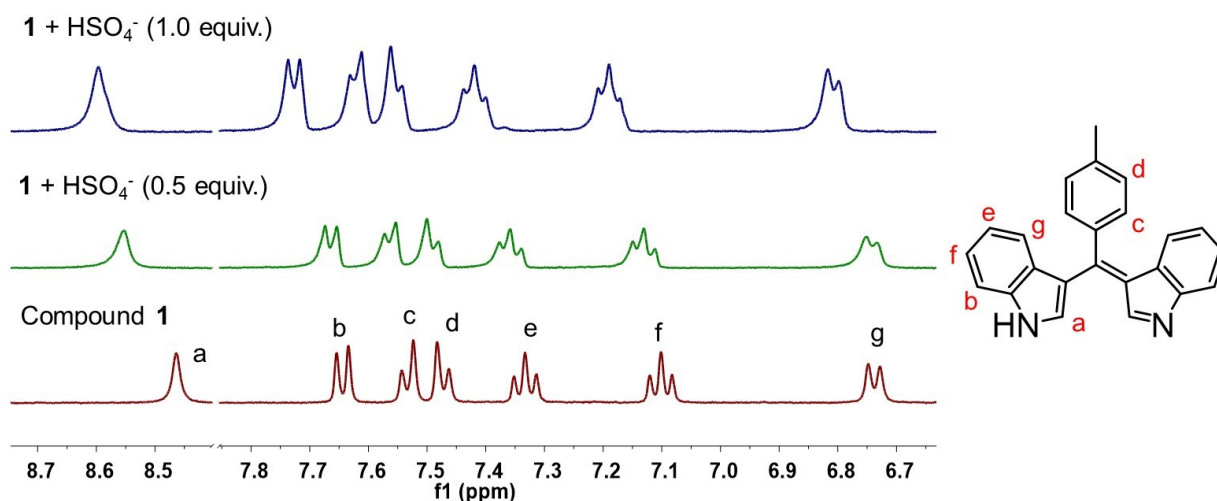**Fig S4.** Partial ^{1}H-NMR spectra of **1** (5 mM) with TBA⁺CN⁻ (0, 0.5 and 1 equiv.) in DMSO-d_6 medium.

Fig S5. Partial ^{1}H-NMR spectra of **1** (5 mM) with TBA$^+$HSO$_4^-$ (0, 0.5 and 1 equiv.) in DMSO-d_6 medium.
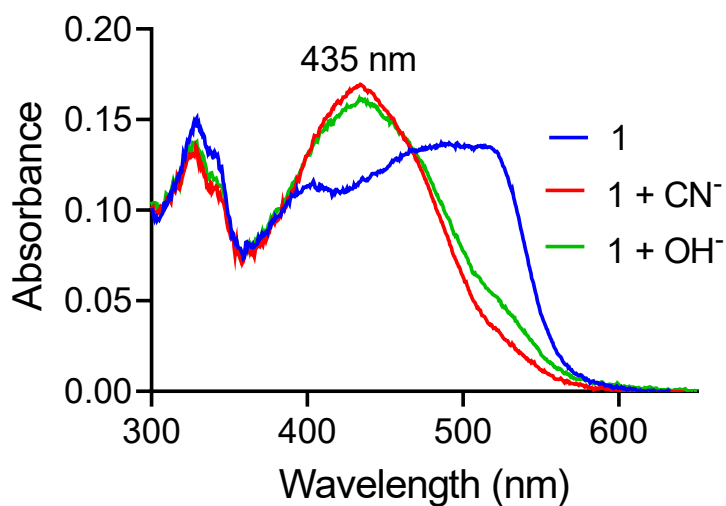

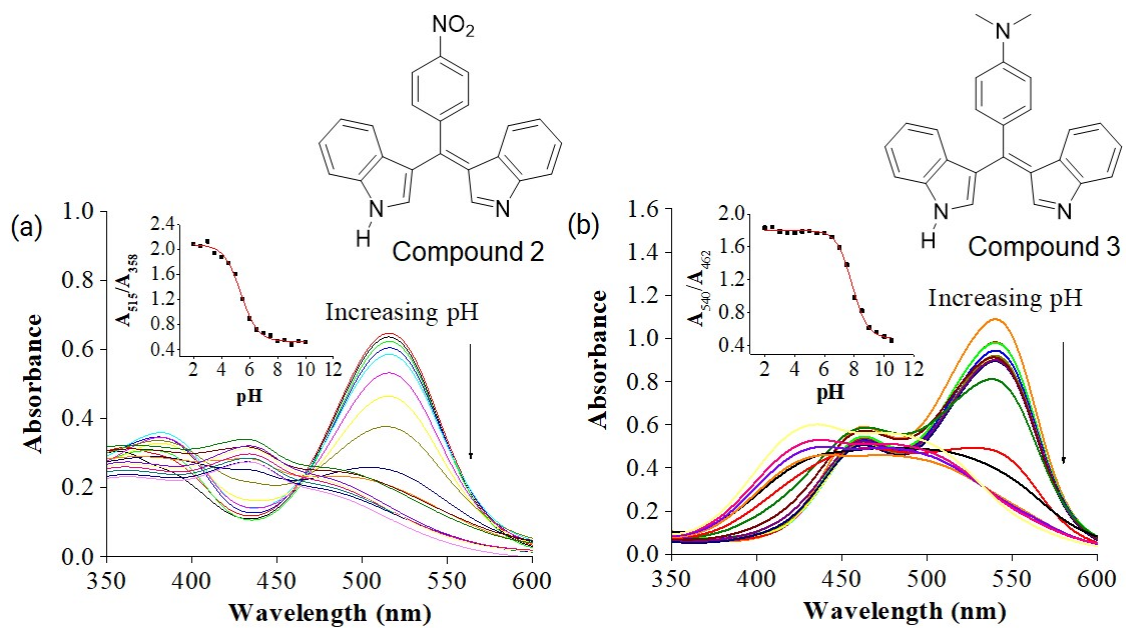**Fig S6.** UV-visible spectra of **1** (10 μM) with CN$^-$ (10 μM) and OH$^-$ (10 μM) in water medium.

Fig S7. (a) UV-visible spectra of **2** (10 µM) at different pH in buffered medium. (b) UV-visible spectra of **3** (10 µM) at different pH in buffered medium.

Computational studies

Table S1: Binding energies of **1**-CN⁻ and **1**-HSO₄⁻ complexes calculated combining DFT/B3LYP theoretical model, 6-311+G*basis set and IEFPCM/Water solvent model.

Probe-anionic complexes	Binding energy, kJ Mol^{-1}
1-CN⁻	-24.82
2-CN⁻	-25.71
3-CN⁻	-24.49
1-HSO₄⁻	-36.46
2-HSO₄⁻	-35.23
3-HSO₄⁻	-38.19

Table S2: Analysis of HOMO-LUMO transition energies of **1**, **2**, **3** and their anionic complexes and decrease of HOMO-LUMO transition energies due to binding with anion, calculated combining DFT/B3LYP theoretical model, 6-311+G*basis set and IEFPCM/Water solvent model.

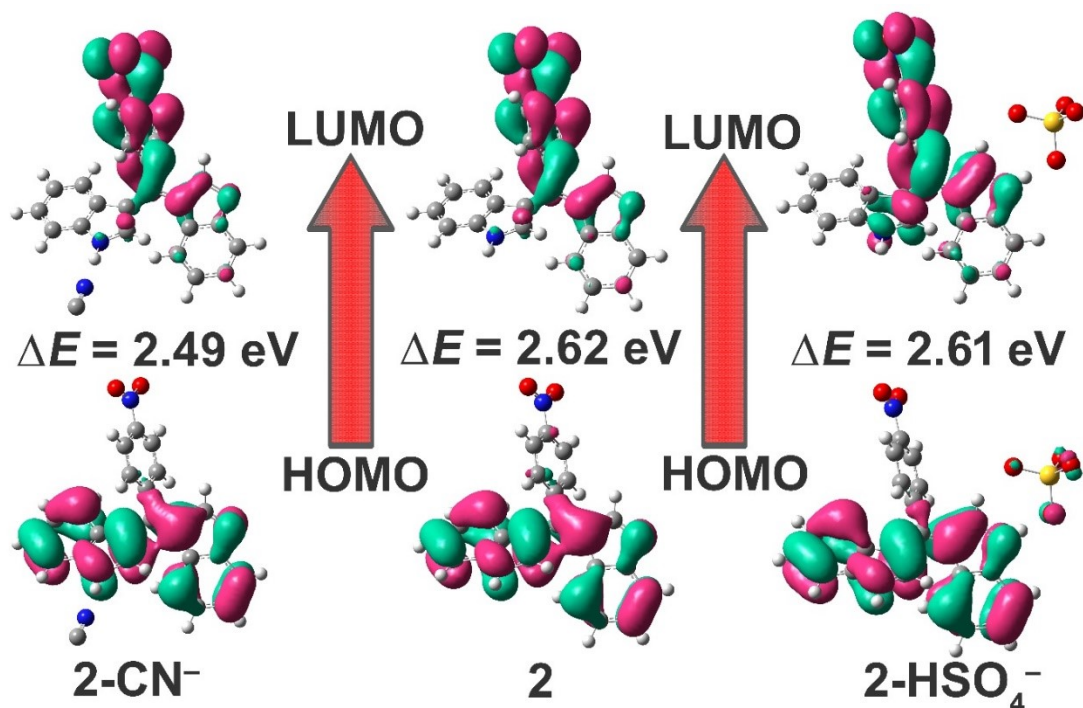| Analytes	ΔE, eV (HOMO-LUMO)	Analytes	Decrease of HOMO-LUMO energy gap [ΔE (Probe-anion) − ΔE (Probe)], eV
1	3.28		
2	2.62		
3	3.05		
1-CN⁻	3.22	(**1**-CN⁻) − **1**	−0.06
2-CN⁻	2.49	(**2**-CN⁻) − **2**	−0.13
3-CN⁻	3.01	(**3**-CN⁻) − **3**	−0.04
1-HSO₄⁻	3.22	(**1**-HSO₄⁻) − **1**	−0.06
2-HSO₄⁻	2.61	(**3**-HSO₄⁻) − **2**	−0.01
3-HSO₄⁻	2.98	(**3**-HSO₄⁻) − **3**	−0.07

Fig. S8. HOMO-LUMO images along with energy gaps for **2**-CN⁻ (left), **2** (middle) and **2**-HSO₄⁻(right) in water medium computed using DFT/B3LYP/6-311+G* theoretical method and IEFPCM solvent model.
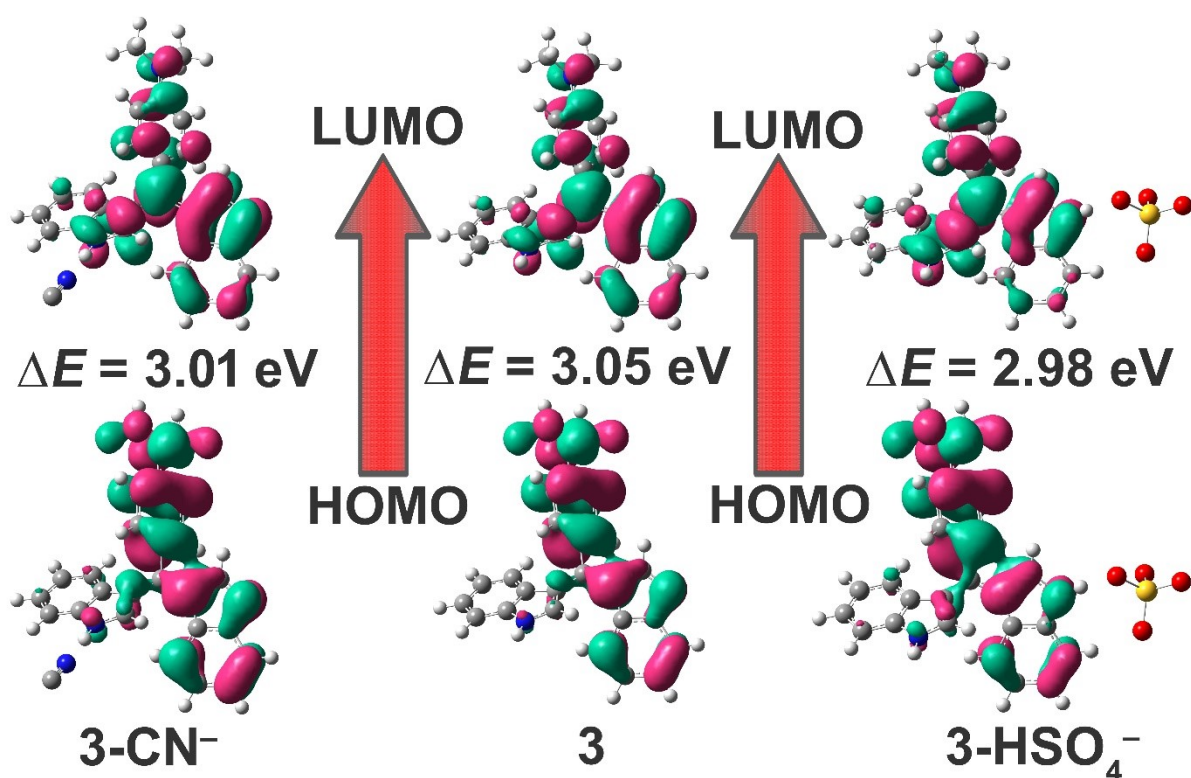

Fig. S9: HOMO-LUMO images along with energy gaps for **3**-CN⁻ (left), **3** (middle) and **3**-HSO₄⁻ (right) in water medium computed using DFT/B3LYP/6-311+G* theoretical method and IEFPCM solvent model.
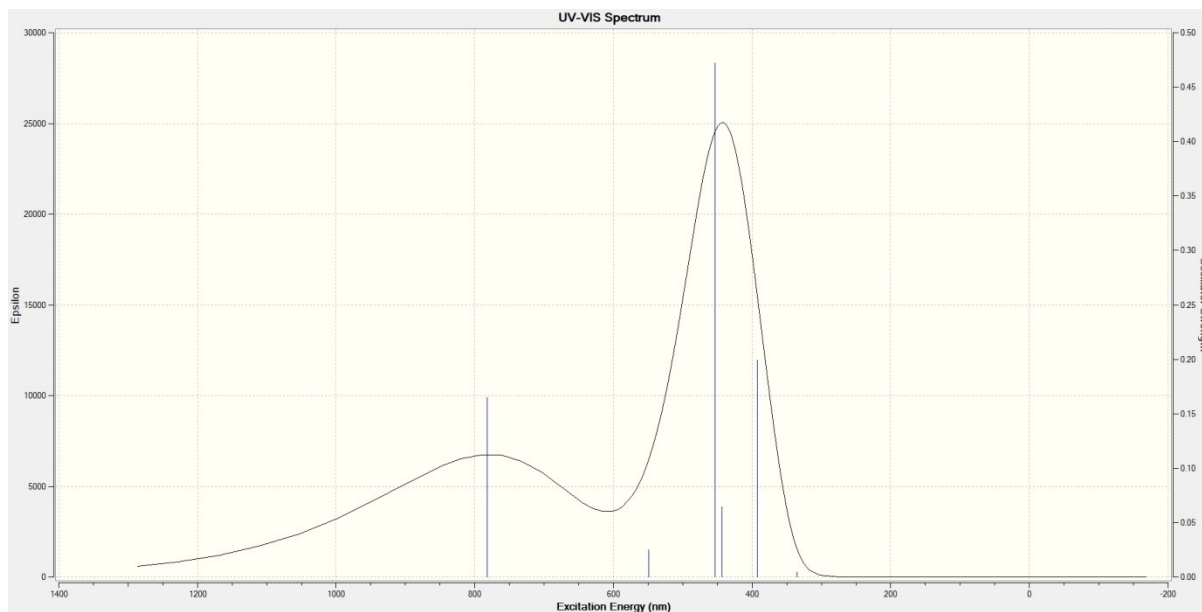
Fig. S10: UV-visible spectra of the anionic form of **1** in water medium computed using TD-DFT/B3LYP/6-311+G* theoretical method and IEFPCM solvent model.
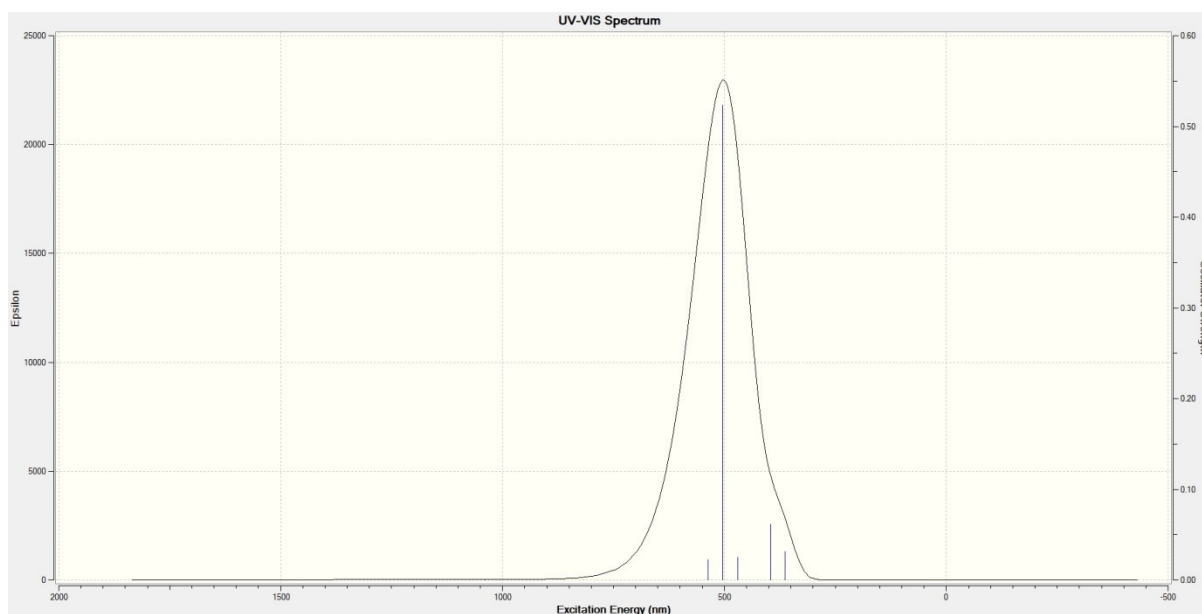

Fig. S11: UV-visible spectra of the cationic form of **1** in water medium computed using TD-DFT/B3LYP/6-311+G* theoretical method and IEFPCM solvent model.
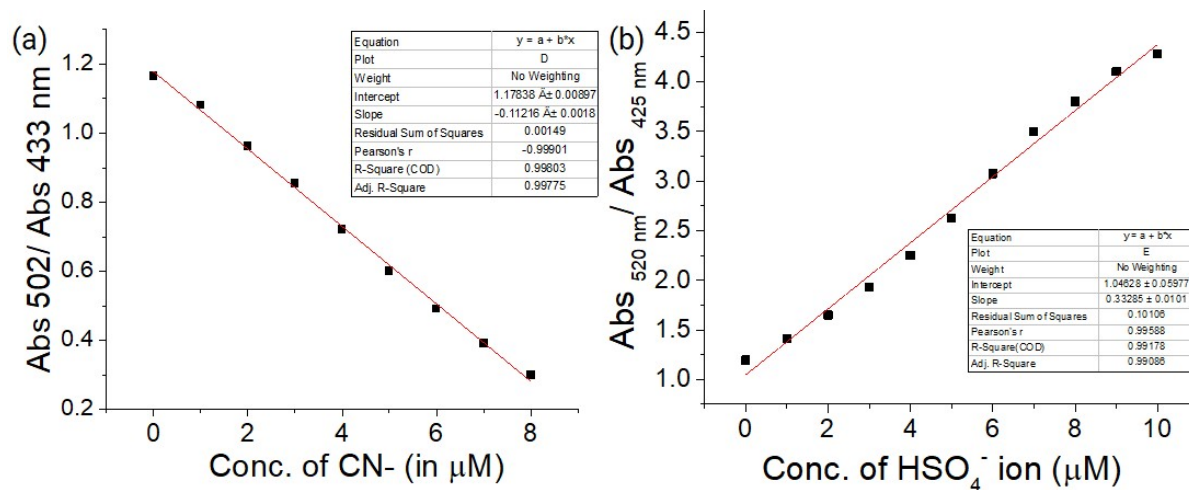
Real-life Sample Analysis

Fig S12. (a) Change in absorbance of **1** (10 µM) with CN¯ in water medium. (b) Change in absorbance of **1** (10 µM) with HSO_4¯ in water medium.
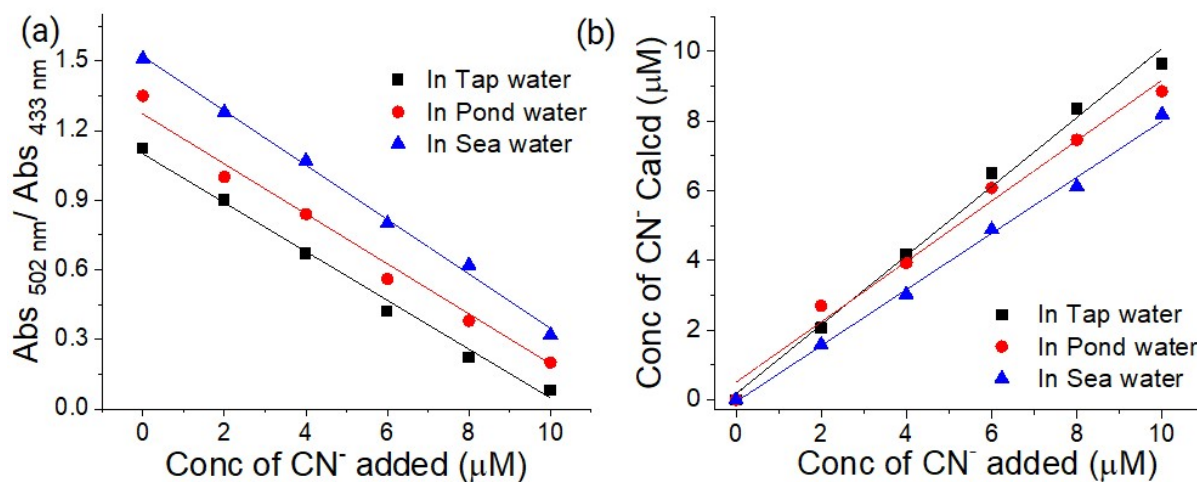

Fig S13. (a) Change in absorbance ratios of **1** (10 µM) with CN¯ in different natural water samples. (b) Recovery plots for CN¯ ions in water medium.

System	HSO_4^- (µM) (present method)	HSO_4^- (µM) (turbidimetric method)	Recovery (%)
DW1	6.48	6.7	103.3
DW2	10.10	10.8	106.5
S1	20.33	21.5	105.5
S2	25.45	26.7	104.7
T1	35.67	37.4	104.3
T2	38.23	39.2	103.2

Table S3. Determination of HSO_4^- in different real-life samples

Reference:

1. S. Jha and N. Dey, ChemistrySelect 2021, **6**, 9211–9216.